Published in final edited form as:
J Neurosci. 2013 January 30; 33(5): 2048–2059. doi:10.1523/JNEUROSCI.3177-12.2013.

Biphasic cholinergic synaptic transmission controls action potential activity in thalamic reticular nucleus neurons

Yan-Gang Sun[1], **Juan D. Pita-Almenar**[1], **Chia-Shan Wu**[2], **John J. Renger**[3], **Victor N. Uebele**[3], **Hui-Chen Lu**[2], and **Michael Beierlein**[1]

[1]Department of Neurobiology & Anatomy, University of Texas Medical School Houston, TX 77030

[2]The Cain Foundation Laboratories Jan and Dan Duncan Neurological Research Institute, Department of Pediatrics Baylor College of Medicine, Houston, TX 77030

[3]Merck Research Laboratories, West Point, PA 19486

Abstract

Cholinergic neurons in the basal forebrain and the brain stem form extensive projections to a number of thalamic nuclei. Activation of cholinergic afferents during distinct behavioral states can regulate neuronal firing, transmitter release at glutamatergic and GABAergic synapses, and synchrony in thalamic networks, thereby controlling the flow of sensory information. These effects are thought to be mediated by slow and persistent increases in extracellular ACh levels, resulting in the modulation of populations of thalamic neurons over large temporal and spatial scales. However, the synaptic mechanisms underlying cholinergic signaling in the thalamus are not well understood. Here, we demonstrate highly reliable cholinergic transmission in the mouse thalamic reticular nucleus (TRN), a brain structure essential for sensory processing, arousal, and attention. We find that ACh release evoked by low-frequency stimulation leads to biphasic excitatory-inhibitory (E-I) postsynaptic responses, mediated by the activation of postsynaptic α4β2 nicotinic (nAChRs) and M2 muscarinic ACh receptors (mAChRs), respectively. In addition, ACh can bind to mAChRs expressed near cholinergic release sites, resulting in autoinhibition of release. We show that the activation of postsynaptic nAChRs by transmitter release from only a small number of individual axons is sufficient to trigger action potentials in TRN neurons. Furthermore, short trains of cholinergic synaptic inputs can powerfully entrain ongoing TRN neuronal activity. Our study demonstrates fast and precise synaptic E-I signaling mediated by ACh, suggesting novel computational mechanisms for the cholinergic control of neuronal activity in thalamic circuits.

Keywords

autoreceptor; desensitization; spillover; minimal stimulation; T-type Ca^{2+} channels; TTA-P2; volume transmission

To whom correspondence should be addressed: Michael Beierlein Department of Neurobiology & Anatomy University of Texas Medical School 6431 Fannin, Suite 7.046 Houston, TX 77030 Tel: 713-500-5619 Fax: 713-500-0621 michael.beierlein@uth.tmc.edu. Y.-G. Sun's present address: Institute of Neuroscience, Chinese Academy of Sciences, Shanghai 200031, China

Conflicts of Interest: V.N.U. and J.J.R. are employees of Merck & Co., Inc. and potentially own stock and/or stock options in the company.

Introduction

Neurons in the thalamic reticular nucleus (TRN) are exclusively GABAergic and project to first and second order thalamic nuclei in the dorsal thalamus (Pinault, 2004; Jones, 2007). TRN is hypothesized to engage in a number of diverse processes, such as sensory information processing (Hartings et al., 2003), attention (Crick, 1984; McAlonan et al., 2006), and the generation of synchronous activity in the thalamocortical system (Kim et al., 1997). However, our understanding of the properties of the various types of inputs contacting TRN neurons, as well as the postsynaptic integration of these inputs in the dendrites of TRN neurons is still limited. Such knowledge is critical to gain a better understanding of the role played by TRN in different types of computational tasks.

TRN neurons are the target of several types of neuromodulatory systems (McCormick, 1989, 1992). Chief among them are cholinergic inputs that originate from two distinct sources, the nucleus basalis of the forebrain and the pedunculopontine and laterodorsal tegmental (PPT and LDT) nuclei of the brainstem. The release of acetylcholine (ACh) from cholinergic afferents is thought to control the firing modes in both TRN and thalamic relay neurons (McCormick and Bal, 1997), primarily by binding to muscarinic acetylcholine receptors (mAChRs), and, to a lesser extent, nicotinic acetylcholine receptors (nAChRs). However, cholinergic control of neuronal excitability has been primarily examined using exogenous agonists and antagonists (Lee and McCormick, 1995) and little is known about the mode of cholinergic signaling under physiological conditions. In vivo work in the TRN has demonstrated short-latency postsynaptic signals in response to stimulation of cholinergic afferents from the brainstem (Hu et al., 1989), consistent with signaling via conventional synapses. However, the majority of release sites formed by cholinergic afferents do not appear to be closely associated with dendrites of TRN neurons (Parent and Descarries, 2008). Furthermore, the changes in membrane potential evoked by cholinergic afferent stimulation can be long-lasting (Hu et al., 1989), consistent with a slow breakdown of ACh far from sites of release. Taken together, this would argue that cholinergic afferent activity in the TRN does not directly engage in precise computational roles, but instead modulates network function on larger temporal and spatial scales, similar to what has been postulated for other brain areas (Descarries et al., 1997).

Our results, obtained using mouse somatosensory thalamic slices, strongly challenge this view. We show that the release of ACh from individual cholinergic axons leads to reliable biphasic excitatory-inhibitory (E-I) responses in TRN neurons, mediated by the rapid activation of postsynaptic nAChRs and mAChRs, respectively. Furthermore, we find that cholinergic inputs activated at 10 Hz can rapidly and reliably entrain TRN neuronal firing. Thus, rather than acting exclusively as a slow neuromodulator, ACh can precisely control postsynaptic activity in individual TRN neurons.

Materials and Methods

Slice preparation

Thalamocortical slices (400 μm) were prepared from both male and female C57BL/6 mice, P13–20, as described previously (Agmon and Connors, 1991). Animals were anesthesized with isofluorane and decapitated, following procedures in accordance with NIH guidelines and approved by the UTHSC-Houston animal welfare committee. Slices were cut in an ice-cold sucrose-containing solution consisting of (in mM) 234 sucrose, 2.5 KCl, 1.25 NaH_2PO_4, 10 $MgSO_4$, 26 $NaHCO_3$, 10 glucose, and 0.5 $CaCl_2$, saturated with 95% O_2-5% CO_2, using a vibratome (Leica VT1200S, Wetzlar, Germany) at slicing speeds of 0.2 mm/s and a blade vibration amplitude of 0.8 mm. Slices were incubated at 34 °C for 40 min, in

saline solution containing (in mM) 126 NaCl, 26 $NaHCO_3$, 2.5 KCl, 1.25 NaH_2PO_4, 10 glucose, 2 $CaCl_2$, and 2 $MgCl_2$, and then kept at room temperature prior to recordings.

Electrophysiology

Slices were placed on glass coverslips coated with poly-L-lysine (Sigma, St. Louis, MO), and submerged in a recording chamber (Warner Instruments, Hamden, CT). All experiments were performed at 32–34°C using an in-line heater while perfusing the recording chamber with solution at 3–4 ml/min using a Minipulse 3 pump (Gilson, Middleton, WI). Unless noted, experiments were carried out in the presence of NBQX (10 μM), 3-((*R*)-2-Carboxypiperazin-4-yl)-propyl-1- phosphonic acid (R-CPP, 5 μM), picrotoxin (50 μM) and CGP 55845 (5 μM) to block AMPA, NMDA, $GABA_A$, and $GABA_B$ receptors, respectively. Recordings were obtained under IR-DIC visualization using an Olympus BX51WI microscope (Olympus Optical, Tokyo, Japan) and a CCD camera (Hamamatsu, Hamamatsu City, Japan).

For whole-cell voltage-clamp recordings, recording pipettes were filled with an internal solution containing the following (in mM): 120 $CsMeSO_3$, 10 CsCl, 10 HEPES, 11 EGTA, 1 $MgCl_2$, 1 $CaCl_2$, 2 Mg-ATP, 0.3 Na-GTP, and 1 QX-314, adjusted to 295 mOsm and pH 7.3. Whole-cell current-clamp recordings from TRN neurons were obtained with an internal solution containing (in mM): 108 KGluc, 26 KCl, 10 HEPES, 0.5 EGTA, 2 $MgCl_2$, 0.16 $CaCl_2$, 2 Mg-ATP, and 0.4 Na-GTP, adjusted to 295 mOsm and pH 7.3. Loose-patch recordings were obtained in voltage-clamp with pipettes (2–3 MΩ) filled with ACSF, and the seal resistance was 20–100 MΩ. Holding potential was continually monitored and adjusted to keep the holding current near 0 pA, in order to minimize any influence on the membrane potential of the recorded cell (Perkins, 2006). Extracellular stimuli were evoked every 12 s with patch pipettes (5–8 μm, tip diameter) filled with ACSF, placed into the TRN (100–200 μm from the recorded cell). Stimulation intensities ranged from 10–30 μA (200 μs stimulus duration), unless noted otherwise.

Physostigmine, Dihydro-β-erythroidine hydrobromide (DHβE), AF-DX 116, Nicotine ditartrate, Methyllycaconitine citrate (MLA), PNU 120596, R-CPP, NBQX, picrotoxin, and CGP 55845 were purchased from Tocris Cookson (Ellisville, MO). TTA-P2 was obtained from Merck Research Laboratories (West Point, PA). All other chemicals were obtained from Sigma (St. Louis, MO).

Data acquisition and analysis

Data were acquired using pClamp software (Molecular Devices, Sunnyvale, CA). Recordings were filtered at 2–10 kHz and digitized at 20 kHz with a 16-bit analog-to digital converter (Digidata 1440A, Molecular Devices, Sunnyvale, CA). Data analysis was performed with custom macros written in Igor Pro (Wavemetrics, Lake Oswego, OR). Response amplitude variability was measured as the coefficient of variation (CV). Noise-corrected values for the CV were computed as: $SQRT(variance_{signal}\text{-}variance_{noise})/mean_{signal}$. Noise was measured from the baseline just before the stimulation by employing the same fixed time window as for the response. Statistical test were performed with the unpaired or paired Student's t-test. Differences are considered to be significant at $p < 0.05$. Data are presented as mean ± s.e.m.

Immunohistochemistry

The generation, genotyping and characterization of cholinergic neuron reporter mice has been described previously (Tallini et al., 2006). Briefly, transgenic mice were engineered to express eGFP under the control of choline acetyltransferase (ChAT) transcriptional regulatory elements. This was accomplished by introducing a modified bacterial artificial

chromosome (BAC) spanning the endogenous ChAT locus, in which the eGFP cassette was inserted at the initiation codon of the ChAT gene. Immunohistochemical staining was performed as described previously (Wu et al., 2010). Brains were sectioned coronally into 50 μm thick sections with a Leica VT1000S vibrating microtome. Two primary antibodies, rat anti-M2 muscarinic acetylcholine receptor (1:1000, Millipore, Temecula, CA) and chicken anti-GFP (1:2000, Aves Labs, Tigard, OR) were used. Fluorescent signals for M2 muscarinic acetylcholine receptors and GFP were detected by using the secondary antibodies goat anti-rat IgG-Dylight 594 (1:500, Jackson ImmunoResearch Laboratories, West Grove, PA) and goat anti-chicken IgG-Alexa 488 (1:500, Invitrogen, Grand Island, NY), respectively. Confocal images were obtained using a Zeiss 510 system.

Results

Release of ACh elicits EPSCs in TRN neurons by activating α4β2 nAChRs

To examine the mechanisms underlying cholinergic neurotransmission, we performed whole-cell voltage clamp recordings from GABAergic neurons in the thalamic reticular nucleus (TRN), in thalamocortical slices of mice. Experiments were initially carried out in the presence of R-CPP, picrotoxin, and CGP55845 to block NMDARs, $GABA_A$Rs, and $GABA_B$Rs, respectively, and TRN neurons were recorded with a Cs-based internal solution (Fig. 1*A*). Single stimuli applied locally in the TRN led to EPSCs with two distinct components. In the example shown in Fig. 1*B*, the fast EPSC (latency = 1.1 ms, 20–80% rise time = 0.4 ms, decay time constant = 1.6 ms) was blocked by the AMPAR antagonist NBQX, indicating activation of glutamatergic synapses formed by both thalamic and neocortical afferents. The remaining EPSC had much slower kinetics (latency = 3.5 ms, 20–80% rise time = 10.8 ms, decay time constant = 123.6 ms) and was blocked by the nicotinic acetylcholine receptor (nAChR) antagonist dihydro-β-erythroidine (DHβE, 3 μM). Consistently, the non-specific nAChR antagonist hexamethonium (100 μM) also blocked isolated slow EPSCs (Fig. 1*H*). Slow EPSCs were dependent on action potential activity and were completely blocked by TTX (500 nM, Fig. 1*H*). Thus, the release of acetylcholine (ACh) evoked by individual stimuli reliably triggered nAChR-mediated EPSCs (nEPSCs) in TRN neurons. All experiments described below except those shown in Fig. 2 were carried out in the presence of both glutamatergic and GABAergic receptor antagonists to isolate nEPSCs.

Nicotinic AChRs expressed throughout the brain primarily exist as α4β2 heteropentamers or α7 homopentamers (Dani and Bertrand, 2007; Miwa et al., 2011). These two nAChR subtypes are often co-expressed in postsynaptic membranes and display dramatically distinct kinetics and pharmacological properties (Dani and Bertrand, 2007). To determine their relative contribution in mediating the nEPSC in TRN neurons, we employed subtype-specific antagonists and modulators. We found that bath application of 300 nM DHβE, which at this concentration selectively blocks α4β2 nAChRs, largely eliminated nEPSCs (157.6 ± 25.1 pA in control, 13.8 ± 2.7 pA in DHβE, $p < 0.001$, $n = 8$, Fig. 1*C,D,H*). By contrast, the α7 nAChR selective antagonist methyllycaconitine (MLA, 50 nM) only moderately decreased nEPSCs (Fig. 1*H*). Furthermore, bath application of the α7 nAChR specific allosteric modulator PNU 120596 (10 μM), which enhances EPSCs mediated by α7 nAChRs (Hurst et al., 2005), had no effect on nEPSC amplitudes (124.8 ± 18.0 pA in control, 122.4 ± 16.6 pA in PNU 120596, $p = 0.72$, Fig. 1*H*). Compared to α7 nAChRs, α4β2 nAChRs have a relatively high affinity for agonist activation and show substantial desensitization in the presence of low concentrations (< 500 nM) of nicotine (Dani and Bertrand, 2007). We found that bath application of nicotine (100 nM) significantly attenuated nEPSCs (Fig. 1*H*). Taken together, our data indicate that nEPSCs in the TRN are largely if not entirely mediated by activation of α4β2 nAChRs.

The time course of released ACh is controlled by diffusion and breakdown via acetylcholinesterase (AChE). To determine the role of AChE activity in shaping nEPSC kinetics, we applied the AChE inhibitor physostigmine (10 μM), in the presence of atropine to block muscarinic AChRs (mAChRs, see below). Physostigmine significantly prolonged the nEPSC decay time constant (302.2 ± 38.9 ms in control, 2381.4 ± 352.5 ms in physostigmine; $p < 0.01$, $n = 5$, Fig. 1*E–G*), indicating that AChE controls the time course of nAChR activation under physiological conditions. Physostigmine application also led to a significant decrease in nEPSC amplitude (172.8 ± 15.6 pA in control, 77.4 ± 6.1 pA in physostigmine; $p < 0.01$, $n = 5$), likely due to nAChR desensitization caused by increases in ambient ACh levels.

Recent studies have demonstrated the synaptic release of glutamate from cholinergic neurons (Higley et al., 2011; Ren et al., 2011). To test for potential co-release of glutamate and ACh from the same afferents targeting TRN, we performed local stimulation at low frequencies, in the absence of AMPAR antagonists. Assuming that nAChRs and AMPARs are co-expressed at postsynaptic sites and can be reliably activated following transmitter release from the same axons, the stimulus intensity for recruiting fast AMPAR EPSCs and slow nEPSCs should be the same. However, we found that nEPSCs could be evoked in isolation at low stimulus intensities, with increases in stimulus intensity typically leading to the recruitment of a fast AMPAR EPSC (Fig. 2), strongly suggesting that in the TRN, glutamate and ACh are liberated from distinct types of synapses.

Postsynaptic M2 mAChRs mediate stimulus evoked IPSCs

TRN neurons express G_i coupled M2 muscarinic acetylcholine receptors (mAChRs) in their dendrites (Oda et al., 2007), whose activation by exogenously applied ACh leads to membrane hyperpolarization (Lee and McCormick, 1995). However, the dynamics of their activation under physiological conditions are not well understood. In neurons throughout the brain mAChRs are thought to be expressed extrasynaptically (Yamasaki et al., 2010) and to respond to slow and widespread increases in extracellular ACh levels, evoked by sustained activation of cholinergic inputs. To explore the conditions leading to the activation of TRN mAChRs, neurons were recorded in voltage clamp with a K-based internal solution. Surprisingly, we found that single stimuli in the TRN evoked biphasic excitatory-inhibitory (E-I) postsynaptic responses, with an early EPSC followed by a late IPSC (Fig. 3*A*). As demonstrated above, the EPSC was mediated by nAChR activation and was blocked by DHβE (3 μM). The remaining IPSC had a slow time course (latency = 31.7 ± 2.6 ms, 20–80% rise time = 107.6 ± 8.6 ms, decay time constant = 639.0 ± 102.0 ms, $n = 5$) and was largely blocked by the mAChR antagonist atropine (10 μM, 40.8 ± 3.3 pA in control, 7.6 ± 2.1 pA in atropine, $p < 0.01$, $n = 5$, Fig. 3*H*) and by the selective M2 mAChR antagonist AF-DX 116 (10 μM, 40.8 ± 9.2 pA in control, 7.2 ± 2.4 pA in AF-DX 116, $p < 0.01$, $n = 7$, Fig. 3*H*). E-I responses could be detected in all cells examined and while the relative contribution of EPSC and IPSC charge to the compound response varied between individual neurons, most responses were dominated by the IPSC (average E/I ratio = 0.54±0.19, median E/I ratio = 0.26, n=17, Fig. 3*B*). We found that isolated muscarinic IPSCs (muIPSCs) reversed at −93.2 ± 0.6 mV ($n = 6$) and displayed a moderate inward rectification (Fig. 3*C,D*), indicating the opening of a K^+ conductance triggered by M2 mAChR activation. Furthermore, muIPSCs significantly curtailed nAChR-mediated excitation, which could be blocked by bath application of AF-DX 116 (Fig. 3*E,F*, left panels). By contrast, AF-DX 116 did not change the decay of the nEPSC when postsynaptic K^+ conductances were blocked by recording TRN neurons with Cs-based internal solution (Fig. 3*E,F*, right panels). Taken together, these data show that the release of ACh in response to single stimuli can lead to an E-I postsynaptic response, mediated by the

activation of nAChRs and the opening of a K^+ conductance, triggered by mAChR activation, respectively.

We performed additional experiments to characterize the nature of the K^+ conductance linked to mAChR activation. The rectification observed for the muIPSC (Fig. 3*C,D*) is consistent with the opening of a G-protein coupled inwardly rectifying potassium (GIRK) conductance (Luscher et al., 1997). In agreement, muIPSCs rapidly attenuated when neurons were dialyzed with an internal solution containing GDPβS (1 mM) to block postsynaptic G protein activation (Fig. 3G,*H*). Furthermore, bath application of either barium (200 μM) or the selective GIRK antagonist Tertiapin-Q (200 nM) largely blocked muIPSCs (Fig. 3H). Taken together, our data suggest that M2 mAChR activation by synaptically released ACh leads to the opening of GIRK conductances in TRN neurons.

Release of ACh from individual cholinergic axons activates both nAChRs and mAChRs

While our findings described above clearly demonstrate the existence of fast cholinergic signaling in the TRN, it is possible that the simultaneous activation of many afferents is required to generate postsynaptic responses, raising concerns about their physiological significance. To quantify the impact of ACh release from individual axons, we employed minimal stimulation techniques. We first characterized unitary nEPSCs, using a Cs-based internal solution. Stimulus intensity was adjusted, so that single stimuli evoked a roughly equal number of response failures and successes (Fig. 4*A,B*). Amplitude variability of successful trials was extremely low, suggesting the activation of individual axons. For the experiment shown, a small increase in stimulus intensity completely eliminated all response failures, but did not lead to a significant change in the average amplitude of successes (92.5 pA at 6.5 μA, 94.9 pA at 9.0 μA, Fig. 4*B*), indicating that additional synaptic inputs were not recruited. Thus, the large majority of response failures observed at lower stimulus intensities likely resulted from a failure of axonal stimulation, rather than a failure of transmitter release. Similar findings were made for 5 additional unitary inputs (Fig. 4*C*). While response amplitudes of unitary synaptic inputs varied between cells (46.7 ± 11.8 pA, ranging from 19.1 to 92.5 pA, n = 6, Fig. 4*C*, left), the coefficient of variation was generally low (0.10 ± 0.01, ranging from 0.05 to 0.14, n = 6), and not a single unitary input displayed failures of release (Fig. 4*C*, right). These data suggest that ACh release from single cholinergic axons can trigger large postsynaptic nAChR-dependent responses, mediated at least in part by a high synaptic release probability.

To determine if release of ACh from individual axons can reliably activate both nAChRs and mAChRs, we performed minimal stimulation experiments for cells recorded with a K-based internal solution. We found that nEPSCs and muIPSCs evoked at threshold intensities co-varied in their successes and failures, i.e. stimuli evoked either a biphasic response or no response at all (Fig. 4*D,E*). Importantly, E-I signaling was observed in all minimal stimulation experiments. While the stimulus intensity required to activate a unitary cholinergic input at threshold was quite variable for different neurons, it was identical for nEPSCs and muIPSCs in a given neuron (Fig. 4*F*). Thus, E-I signaling mediated by the activation of postsynaptic nAChRs and mAChRs is present even at the level of individual inputs.

The experiments described above were aimed to isolate individual cholinergic afferents. To test whether multiple cholinergic axons form functional synapses with individual TRN neurons, we performed recordings using a Cs-based internal solution and measured nEPSC amplitudes evoked by a range of stimulus intensities. As shown for a representative recording (Fig. 4*G,H*), we found that increases in stimulus intensity resulted in a stepwise increase in nEPSC amplitude, suggesting the recruitment of additional axons at higher

stimulus intensities. Similar findings were made in 4/4 additional experiments. Thus, individual TRN neurons receive convergent input from several distinct cholinergic axons.

Autoinhibition of ACh release is mediated by presynaptic M2 mAChRs

Transmitter release during ongoing synaptic transmission is often under the control of negative feedback mechanisms mediated by metabotropic autoreceptors (Deisz and Prince, 1989; Scanziani et al., 1997). The presence of mAChRs near sites of release could allow for autoinhibition of ACh signaling. To test for the existence of mAChRs on cholinergic afferents, we recorded nEPSCs in the TRN using a Cs-based internal solution, prior to and following bath application of low doses of muscarine (Fig. 5*A–C*). Muscarine (1 μM) caused a strong reduction in nEPSC amplitude, which was reversed by the application of the M2 mAChR antagonist AF-DX 116 (10 μM, 19.7 ± 8.4% of control in muscarine, 96.1 ± 3.9% of control in AF-DX 116, n = 5), suggesting that cholinergic afferents express M2 mAChRs near sites of release.

Next, we examined the activation of presynaptic mAChRs via synaptically released ACh, by activating cholinergic afferents using paired-pulses (0.1–5 Hz), prior to and following application of the M2 mAChR antagonist AF-DX 116 (10 μM, Fig. 5*D,E*). In control conditions, nEPSCs displayed paired-pulse depression ($nEPSC_2/nEPSC_1$ = 0.41 ± 0.05 at 2 Hz, n = 5). Following AF-DX 116 application, the amplitude of $nEPSC_1$ remained unchanged (93.6 ± 3.0% of control in AF-DX 116, n = 5), showing that in control conditions release probability was not modulated by ambient levels of ACh (Fig. 5*D,E*). By contrast, the amplitude of $nEPSC_2$ increased by 53.1±18.4% (n = 5), leading to a significant increase in paired-pulse ratio ($nEPSC_2/EPSC_1$ = 0.41 ± 0.05 in control, 0.63 ± 0.03 in AF-DX 116, n = 5, $p < 0.001$). Changes in paired-pulse ratio following AF-DX 116 application were detected up to an ISI of 1 s (Fig. 5*F*). To rule out a postsynaptic mechanism for the M2 mAChR antagonist-induced change in paired-pulse plasticity, we repeated these experiments while blocking postsynaptic G protein signaling by adding GDPβS (1 mM) to the internal solution. Under these conditions, blocking M2 mAChRs by bath application of AF-DX 116 still led to a significant increase in paired-pulse ratio ($nEPSC_2/EPSC_1$ = 0.36 ± 0.02 in control, 0.51 ± 0.03 in AF-DX 116, n = 5, $p < 0.01$), suggesting that M2 mAChR-mediated changes in paired-pulse plasticity are largely if not entirely presynaptic.

To provide independent evidence for the existence of M2 mAChRs on cholinergic axons we performed immunostaining for M2 mAChRs in brain sections of mouse, which express GFP in choline acetyltransferase (ChAT) containing neurons (Tallini et al., 2006). Abundant M2 mAChR staining was observed in TRN (Fig. 5*G,H*), while the ventrobasal thalamus was largely devoid of M2 mAChR positive signal (Fig. 5*G,H*). Axonal processes containing GFP (green, Fig. 5*I1,J1*) often colocalized with punctate M2 mAChR staining (red, Fig. 5*I2,J2*), strongly suggesting the presence of M2 mAChR on cholinergic axons. Collectively, our data indicate that ongoing cholinergic synaptic transmission is strongly controlled by autoinhibition, mediated by the activation of presynaptic M2 mAChRs.

Pre- and postsynaptic M2 mAChRs control nAChR-mediated postsynaptic excitation during stimulus trains

Having established the activation of both pre- and postsynaptic M2 mAChRs by ACh following single stimuli, we next quantified their role in regulating nAChR-mediated excitation during short stimulus trains, at frequencies (5–10 Hz) within the range of cholinergic neuronal activity observed in vivo (Boucetta and Jones, 2009). We first examined the role of presynaptic M2 mAChRs in isolation, by recording from TRN neurons using a Cs-based internal solution to block IPSCs mediated by postsynaptic M2 mAChRs. In control conditions, nEPSCs showed a moderate short-term depression of stimulus evoked

charge flow (5 Hz, Fig. 6*A,B*). Application of the M2 mAChR antagonist AF-DX 116 (10 μM) led to a significant reduction of this depression, confirming that autoinhibition via presynaptic M2 mAChRs regulates the nAChR dependent postsynaptic excitation during stimulus trains. To estimate the combined effect of both pre- and postsynaptic M2 mAChR activation, we repeated these experiments using a K-based internal recording solution. In control conditions nAChR evoked excitation was rapidly curtailed during a 5-Hz stimulus train, resulting in a net outward current at steady-state (Fig. 6*C,D*, top panels). Following bath application of the M2 mAChR antagonist AF-DX 116 to block pre- and postsynaptic M2 mAChRs, short-term depression of charge flow was entirely eliminated. Similarly, for 10-Hz stimulus trains, nAChR-mediated EPSCs were almost completely depressed at steady-state in control conditions (Fig. 6*C,D*, bottom panels). Bath application of AF-DX 116 completely eliminated depression and revealed slight facilitation of charge flow. These data indicate that activation of both pre and postsynaptic M2 mAChRs leads to a rapid and powerful reduction of nAChR-evoked excitation during ongoing cholinergic activity.

Cholinergic synaptic inputs trigger action potentials in TRN neurons

Having established that activation of cholinergic fibers induces reliable postsynaptic EPSCs by activating nAChRs, we next examined the impact of cholinergic inputs on TRN neuronal firing. We first performed recordings in cell-attached mode (Perkins, 2006) to minimize perturbations of the intracellular milieu. As shown for a representative experiment (Fig. 7*A*), single stimuli reliably triggered spike bursts in TRN neurons, which were completely eliminated following bath application of the nAChR antagonist DHβE (300 nM). Synaptically evoked bursting was observed in all cells examined (4.9 ± 0.6 spikes, 26.3 ± 2.9 ms latency, n = 10), and was completely blocked by DHβE (5.1 ± 1.1 spikes in control, 0 spikes in DHβE, n = 5, $p < 0.01$, Fig. 7*B*). To estimate the amplitude of nAChR-mediated postsynaptic currents necessary to generate action potentials, we recorded from neurons using a Cs-based internal solution (Fig. 7*C*). Neurons were first recorded in cell-attached voltage clamp and stimulus intensity was adjusted so that individual stimuli reliably triggered bursts of action potentials (Fig. 7*C*, top). Following establishment of whole-cell configuration, isolated nEPSCs were evoked using the same stimulus intensity (Fig. 7*C*, bottom). EPSCs had an average amplitude of 152.6 pA (range of 93.4 - 263.7 pA, n = 5), and were completely blocked by DHβE (Fig. 7*C*, bottom). Given our estimates of 46.7 pA for an average unitary nEPSC response (Fig. 4*C*), these data indicate that on average the simultaneous activation of 3.2 individual cholinergic inputs can trigger action potentials in TRN neurons.

TRN neuronal dendrites express T-type Ca^{2+} channels whose activation contributes to the generation of burst firing from a relative hyperpolarized membrane potential (Huguenard and Prince, 1992). To test if T-type Ca^{2+} channel activation is critical for cholinergic input-induced action potential generation, we performed cell-attached recordings from TRN neurons, and bath-applied the specific T-type Ca^{2+} channel blocker TTA-P2 (Dreyfus et al., 2010). We found that synaptically evoked bursting was completely blocked following bath application of TTA-P2 (1 μM, 4.7 ± 0.5 spikes in control, 0 spikes in TTA-P2, n = 5, $p < 0.01$, Fig. 7*D,E*). In principle, the block of synaptically evoked bursting by TTA-P2 could be due to a reduction of ACh release following block of presynaptic T-type Ca^{2+} channels. However, TTA-P2 had no effect on nEPSC amplitude (112.8 ± 27.8 pA in control, 106.9 ± 25.8 pA in TTA-P2, n = 5, p = 0.14, Fig. 7*F*), indicating that T-type Ca^{2+} channels are not involved in triggering release of ACh. Thus, the activation of postsynaptic T-type Ca^{2+} channels is critical for cholinergic input-induced burst firing.

Neurons in the TRN can generate action potentials in either burst mode or tonic mode (Llinas and Jahnsen, 1982), mediated by changes in resting membrane potential associated with different behavioral states. We tested how membrane potential influences action

potential generation evoked by cholinergic synaptic inputs. TRN neurons were recorded in whole-cell mode and held in either burst mode (−70 mV) or tonic mode (−60 mV). In the example shown in Fig. 7*G*, stimulus intensity was adjusted to elicit postsynaptic responses in roughly 50% of all trials, suggesting threshold activation of a single axon. Activation of this input reliably triggered bursts of action potentials when the cell was held at −70 mV, but only single spikes if the resting potential of the postsynaptic neuron was set to −60 mV. Similar results were obtained from 6 additional neurons (3.8 ± 0.3 spikes in burst mode, 1.1 ± 0.1 spikes in tonic mode, n = 7, $p < 0.001$, Fig. 7*H*). Thus, cholinergic input-evoked action potential activity is determined by the membrane potential of the postsynaptic TRN neuron.

Cholinergic synaptic inputs entrain TRN neuronal activity

Next, we tested the impact of brief trains of cholinergic synaptic activity (10 stimuli, 10 Hz) on TRN neuronal firing. For a holding potential of −60 mV, train stimuli evoked a transient postsynaptic depolarization, which gave rise to a long-lasting hyperpolarization following the end of the stimulus train (Fig. 8*A*, top). We then paired stimulus trains with action potential activity evoked by applying long depolarizing current steps (6s, 100–140 pA) to the postsynaptic neuron (Fig. 8*A*, bottom). Cholinergic activity led to a brief increase in TRN neuronal firing at the onset of synaptic stimulation. Following this initial increase, synaptic inputs reduced action potential activity compared to baseline levels (16.6 ± 2.8 Hz in control, 8.5 ± 1.4 Hz during train stimulation, n = 5). Following the end of the stimulus train, spike firing was further reduced (6.2 ± 1.8 Hz, n=5) before returning to baseline levels within 1–2 seconds (time constant of recovery = 528 ± 205 ms, n=5). Interestingly, synaptic stimulation tightly entrained spike firing, such that spike probability peaked within a 20 ms window following individual synaptic stimuli (Fig. 8*B*). Across all neurons examined (n=5), spike probability prior to synaptic stimulation was 0.34 ± 0.06 (bin size = 20 ms). For the last five stimuli of the stimulus train, spike probability immediately following each synaptic stimulus (0–20 ms) was 0.42 ± 0.12, before dropping to 0.09 ± 0.02 (40–60 ms).

To better understand the role of nAChR and mAChR activation in controlling TRN firing, we performed experiments in which each receptor type was blocked individually. Blocking postsynaptic nAChRs via bath application of DHβE (3 μM) dramatically reduced action potential activity during the stimulus train compared to control, resulting in long pauses of spike firing (Fig. 8*C*, n = 3). By contrast, when both pre- and postsynaptic mAChRs were blocked by bath applying AF-DX 116, spike firing moderately increased during synaptic stimulation, but spike entrainment to synaptic activity was no longer apparent (Fig. 8*D*, n = 2). Taken together, these data suggest that the combined activation of nAChRs and mAChRs during cholinergic afferent activity at physiologically realistic rates can lead to the precise entrainment of TRN neuronal firing.

Discussion

An increasing number of studies have shown that cholinergic synaptic transmission mediated by nAChRs is more prominent than previously appreciated (Zhang et al., 1993; Hatton and Yang, 2002; English et al., 2011; Letzkus et al., 2011; Arroyo et al., 2012). Here we demonstrate that in the TRN cholinergic synaptic signaling is mediated by the activation of both nAChRs and mAChRs, leading to E-I postsynaptic responses. Synaptically released ACh also activates presynaptic mAChRs, thereby controlling cholinergic signaling during ongoing activity via autoinhibition. In addition, we show that even a small number of cholinergic afferents can trigger spike activity in postsynaptic TRN neurons. Furthermore, we find that brief trains of cholinergic synaptic activity can reliably entrain TRN neuronal firing. Our findings highlight several novel mechanisms underlying cholinergic transmission in the mammalian central nervous system.

Properties of cholinergic synaptic transmission in the TRN

Our demonstration of reliable cholinergic responses in TRN neurons evoked by individual stimuli is in agreement with the idea that ACh signaling occurs via conventional synapses. This is supported by previous anatomical work demonstrating the existence of ultrastructurally defined synaptic contacts formed by cholinergic afferents, in particular on distal dendrites of TRN neurons (Hallanger and Wainer, 1988; Parent and Descarries, 2008). The functional expression of both nAChRs and mAChRs in TRN dendrites has been known for some time (McCormick and Prince, 1986; Lee and McCormick, 1995). However, the spatial relationship of presynaptic cholinergic terminals and postsynaptic cholinergic receptors is not well understood. Our data indicate that release of ACh from individual axons activates nAChRs and mAChRs co-expressed in the postsynaptic membrane, although we cannot rule out that TRN neurons express only nAChRs or mAChRs near individual release sites. We found that nEPSCs evoked by stimulation of individual axons display relatively large average amplitudes, with unusually low amplitude variability from trial-to-trial, and a complete lack of response failures. This argues that individual afferents contact a given postsynaptic neuron via a large number of release sites, and that release probability p is high, at least during low stimulus frequencies.

While our results are most readily explained by cholinergic signaling via conventional synapses, other forms of non-synaptic fast signaling cannot be excluded (Szapiro and Barbour, 2007; Sarter et al., 2009). The expression of AChE relative to sites of ACh release is not known, so it is possible that synaptically released ACh can diffuse and act on more distant sites prior to its degradation. Such a scenario seems to be supported by a slightly longer response latency as compared to the one of the AMPAR-mediated EPSC, a slow nEPSC rise time, and a low nEPSC amplitude variability from trial-to-trial (c.f. Szapiro and Barbour, 2007). However, the fact that postsynaptic cholinergic responses can be detected following single stimuli applied to individual presynaptic axons places significant constraints on the synaptic ultrastructure underlying cholinergic signaling.

The presence of fast cholinergic signaling does not exclude a role of slower, more widespread forms of signaling. The majority of cholinergic terminals found in TRN do not form synaptic contacts with dendritic processes (Parent and Descarries, 2008). It is possible that release from such terminals as well as from conventional release sites, especially following sustained high-frequency afferent activity, leads to a spatially more widespread and longer lasting ACh signal, leading to the activation of more distant targets such as extrasynaptic cholinergic receptors expressed in dendrites, or receptors expressed in nearby glutamatergic or GABAergic presynaptic terminals and axons (Kawai et al., 2007).

Spike generation by cholinergic inputs

We found that the activation of cholinergic inputs is sufficient to generate action potentials in TRN neurons. Given our estimates of both unitary synaptic responses as well as synaptic response amplitudes sufficient to trigger action potential firing, we estimate that the number of unitary inputs necessary to trigger action potentials is 3.2 on average, arguing that cholinergic input-induced spike generation is a physiologically realistic mechanism.

When TRN neurons were held in burst mode, cholinergic input-evoked spike generation required activation of postsynaptic T-type Ca^{2+} channels, as burst activity was completely eliminated by a T-type Ca^{2+} channel blocker. This extends our previous findings demonstrating that intra-TRN GABAergic synapses generate $GABA_A$ receptor-mediated depolarizations in TRN neurons, which like nEPSPs are amplified by T-type Ca^{2+} channel activation to generate bursts of action potentials (Sun et al., 2012). Anatomical studies have shown that cholinergic synapses target the distal dendrites of TRN neurons, which show

strong expression of T-type Ca^{2+} channels (Crandall et al., 2010). Our data therefore suggest that nEPSPs initiate local Ca^{2+} spikes in TRN dendrites, which then spread towards the Na^{+} spike initiation zone in the axon.

E-I signaling mediated by ACh release

The central finding of our study is that release of ACh from individual axons leads to the reliable activation of both ionotropic and metabotropic ACh receptors and the generation of a biphasic response, in which excitation, mediated by nAChR opening, is followed by inhibition, mediated by opening of GIRK conductances linked to mAChR activation. Importantly, both excitation and inhibition are evoked by the same low-frequency afferent input. Cholinergic E-I signaling with similar stimulus requirements has been previously demonstrated in several systems, such as cholinergic synapses onto interneurons in Aplysia (Blankenship et al., 1971), transient feedback projections to inner hair cells in the neonatal mammalian cochlea (Glowatzki and Fuchs, 2000), and afferent inputs to the superior cervical ganglion (Yarosh et al., 1988). Few well-documented reports exist for other neurotransmitter systems. Glutamate, in addition to evoking fast excitation by binding to ionotropic receptors, can generate an inhibitory response at synapses in the midbrain (Fiorillo and Williams, 1998) and olfactory bulb (Isaacson and Murphy, 2001), triggered by the activation of metabotropic glutamate receptors and NMDA receptors, respectively. Notably, in these cases, the generation of the inhibitory response requires sustained afferent activity, suggesting that transmitter pooling and spillover from the synaptic cleft are necessary to activate extrasynaptically expressed receptors.

What are the functional roles of E-I signaling in the TRN? Although preliminary, our data (Fig. 8) strongly indicate that brief trains of cholinergic afferent activity can lead to the rapid and precise entrainment of TRN neuronal firing. It is likely that neighboring TRN neurons share common input from a number of individual cholinergic axons. TRN neurons form local clusters interconnected by electrical synapses (Long et al., 2004), which have low-pass filter properties and therefore seem well suited to propagate slow signals generated by postsynaptic nAChR and mAChR activation. Thus, cholinergic afferent activity during periods of arousal could play a role in transiently synchronizing local TRN neuronal firing.

More generally, E-I signaling is likely critical for the rapid and precise control of the postsynaptic integration of glutamatergic and GABAergic synaptic inputs in TRN dendrites. For example, glutamatergic EPSPs generated within ~100 ms following cholinergic synapse activation will summate with the nEPSP, enhancing the likelihood of triggering an action potential. For glutamatergic input arriving between ~150 and 1500 ms following cholinergic synapse activation (i.e. during the muIPSP), the effect could be more complex. Opening of GIRK conductances following mAChR activation enhances membrane conductance, which will effectively shunt weak glutamatergic inputs. However, GIRK opening will also lead to a strong de-inactivation of T-type Ca^{2+} channels by hyperpolarizing distal dendrites. Thus, strong glutamatergic inputs which under control conditions only trigger individual spikes will likely trigger bursts of action potentials, due to activation of T-type Ca^{2+} channels from a hyperpolarized membrane potential (McCormick and Prince, 1986). In this way, muIPSPs might create precise temporal windows, during which glutamatergic inputs are differentially processed in TRN dendrites, depending on their strength. Such a role of postsynaptic M2 mAChRs in controlling spike generation is consistent with a previous finding showing that pharmacological activation of M2 mAChRs in thalamic GABAergic interneurons can control spike generation, depending on the strength of sensory input (Antal et al., 2010). More generally, the relative timing of glutamatergic and cholinergic inputs might determine distinct forms of heterosynaptic plasticity, as has been shown for cholinergic and glutamatergic synapses in the hippocampal CA1 region (Gu and Yakel, 2011).

Previous work examining the role of ACh in the thalamus has emphasized long-lasting and widespread changes in membrane excitability and transmitter release, mediated by diffuse transmission and slow changes in the ambient levels of ACh. In marked contrast to this view, our study highlights the presence of rapid and precise cholinergic signaling in the TRN. Future studies will address if such forms of cholinergic transmission exist in other thalamic nuclei.

Acknowledgments

We thank Drs. Adam Carter and Jay Gibson for comments on a previous version of the manuscript, the Baylor IRDDRC core facility (NIH HD024064) for confocal microscopy access, and Dr. Tibor Harkany for providing us with brain tissue of cholinergic neuron reporter mice. This work was supported in part by funds from DA029381 (NIDA) and HD065561 (NICHD) to H-C.L., and NS077989 (NINDS), the American Heart Association, the Whitehall Foundation, and the Epilepsy Foundation to M.B.

References

Agmon A, Connors BW. Thalamocortical responses of mouse somatosensory (barrel) cortex in vitro. Neuroscience. 1991; 41:365–379. [PubMed: 1870696]

Antal M, Acuna-Goycolea C, Pressler RT, Blitz DM, Regehr WG. Cholinergic activation of M2 receptors leads to context-dependent modulation of feedforward inhibition in the visual thalamus. PLoS Biol. 2010; 8:e1000348. [PubMed: 20386723]

Arroyo S, Bennett C, Aziz D, Brown SP, Hestrin S. Prolonged disynaptic inhibition in the cortex mediated by slow, non-alpha7 nicotinic excitation of a specific subset of cortical interneurons. J Neurosci. 2012; 32:3859–3864. [PubMed: 22423106]

Blankenship JE, Wachtel H, Kandel ER. Ionic mechanisms of excitatory, inhibitory, and dual synaptic actions mediated by an identified interneuron in abdominal ganglion of Aplysia. J Neurophysiol. 1971; 34:76–92. [PubMed: 4322253]

Boucetta S, Jones BE. Activity profiles of cholinergic and intermingled GABAergic and putative glutamatergic neurons in the pontomesencephalic tegmentum of urethane-anesthetized rats. J Neurosci. 2009; 29:4664–4674. [PubMed: 19357291]

Crandall SR, Govindaiah G, Cox CL. Low-threshold Ca2+ current amplifies distal dendritic signaling in thalamic reticular neurons. J Neurosci. 2010; 30:15419–15429. [PubMed: 21084598]

Crick F. Function of the thalamic reticular complex: the searchlight hypothesis. Proc Natl Acad Sci U S A. 1984; 81:4586–4590. [PubMed: 6589612]

Dani JA, Bertrand D. Nicotinic acetylcholine receptors and nicotinic cholinergic mechanisms of the central nervous system. Annu Rev Pharmacol Toxicol. 2007; 47:699–729. [PubMed: 17009926]

Deisz RA, Prince DA. Frequency-dependent depression of inhibition in guinea-pig neocortex in vitro by GABAB receptor feed-back on GABA release. J Physiol. 1989; 412:513–541. [PubMed: 2557431]

Dreyfus FM, Tscherter A, Errington AC, Renger JJ, Shin HS, Uebele VN, Crunelli V, Lambert RC, Leresche N. Selective T-type calcium channel block in thalamic neurons reveals channel redundancy and physiological impact of I(T)window. J Neurosci. 2010; 30:99–109. [PubMed: 20053892]

English DF, Ibanez-Sandoval O, Stark E, Tecuapetla F, Buzsaki G, Deisseroth K, Tepper JM, Koos T. GABAergic circuits mediate the reinforcement-related signals of striatal cholinergic interneurons. Nat Neurosci. 2011; 15:123–130. [PubMed: 22158514]

Fiorillo CD, Williams JT. Glutamate mediates an inhibitory postsynaptic potential in dopamine neurons. Nature. 1998; 394:78–82. [PubMed: 9665131]

Glowatzki E, Fuchs PA. Cholinergic synaptic inhibition of inner hair cells in the neonatal mammalian cochlea. Science. 2000; 288:2366–2368. [PubMed: 10875922]

Gu Z, Yakel JL. Timing-dependent septal cholinergic induction of dynamic hippocampal synaptic plasticity. Neuron. 2011; 71:155–165. [PubMed: 21745645]

Hallanger AE, Wainer BH. Ultrastructure of ChAT-immunoreactive synaptic terminals in the thalamic reticular nucleus of the rat. J Comp Neurol. 1988; 278:486–497. [PubMed: 3230169]

Hartings JA, Temereanca S, Simons DJ. State-dependent processing of sensory stimuli by thalamic reticular neurons. J Neurosci. 2003; 23:5264–5271. [PubMed: 12832551]

Hatton GI, Yang QZ. Synaptic potentials mediated by alpha 7 nicotinic acetylcholine receptors in supraoptic nucleus. J Neurosci. 2002; 22:29–37. [PubMed: 11756485]

Higley MJ, Gittis AH, Oldenburg IA, Balthasar N, Seal RP, Edwards RH, Lowell BB, Kreitzer AC, Sabatini BL. Cholinergic interneurons mediate fast VGluT3-dependent glutamatergic transmission in the striatum. PLoS One. 2011; 6:e19155. [PubMed: 21544206]

Hu B, Steriade M, Deschenes M. The effects of brainstem peribrachial stimulation on perigeniculate neurons: the blockage of spindle waves. Neuroscience. 1989; 31:1–12. [PubMed: 2771051]

Huguenard JR, Prince DA. A novel T-type current underlies prolonged Ca(2+)-dependent burst firing in GABAergic neurons of rat thalamic reticular nucleus. J Neurosci. 1992; 12:3804–3817. [PubMed: 1403085]

Hurst RS, Hajos M, Raggenbass M, Wall TM, Higdon NR, Lawson JA, Rutherford-Root KL, Berkenpas MB, Hoffmann WE, Piotrowski DW, Groppi VE, Allaman G, Ogier R, Bertrand S, Bertrand D, Arneric SP. A novel positive allosteric modulator of the alpha7 neuronal nicotinic acetylcholine receptor: in vitro and in vivo characterization. J Neurosci. 2005; 25:4396–4405. [PubMed: 15858066]

Isaacson JS, Murphy GJ. Glutamate-mediated extrasynaptic inhibition: direct coupling of NMDA receptors to Ca(2+)-activated K+ channels. Neuron. 2001; 31:1027–1034. [PubMed: 11580901]

Jones, EG. The thalamus. 2nd Edition. Cambridge University Press; Cambridge; New York: 2007.

Kawai H, Lazar R, Metherate R. Nicotinic control of axon excitability regulates thalamocortical transmission. Nat Neurosci. 2007; 10:1168–1175. [PubMed: 17704774]

Kim U, Sanchez-Vives MV, McCormick DA. Functional dynamics of GABAergic inhibition in the thalamus. Science. 1997; 278:130–134. [PubMed: 9311919]

Lee KH, McCormick DA. Acetylcholine excites GABAergic neurons of the ferret perigeniculate nucleus through nicotinic receptors. J Neurophysiol. 1995; 73:2123–2128. [PubMed: 7623105]

Letzkus JJ, Wolff SB, Meyer EM, Tovote P, Courtin J, Herry C, Luthi A. A disinhibitory microcircuit for associative fear learning in the auditory cortex. Nature. 2011; 480:331–335. [PubMed: 22158104]

Llinas R, Jahnsen H. Electrophysiology of mammalian thalamic neurones in vitro. Nature. 1982; 297:406–408. [PubMed: 7078650]

Long MA, Landisman CE, Connors BW. Small clusters of electrically coupled neurons generate synchronous rhythms in the thalamic reticular nucleus. J Neurosci. 2004; 24:341–349. [PubMed: 14724232]

Luscher C, Jan LY, Stoffel M, Malenka RC, Nicoll RA. G protein-coupled inwardly rectifying K+ channels (GIRKs) mediate postsynaptic but not presynaptic transmitter actions in hippocampal neurons. Neuron. 1997; 19:687–695. [PubMed: 9331358]

McAlonan K, Cavanaugh J, Wurtz RH. Attentional modulation of thalamic reticular neurons. J Neurosci. 2006; 26:4444–4450. [PubMed: 16624964]

McCormick DA. Cholinergic and noradrenergic modulation of thalamocortical processing. Trends Neurosci. 1989; 12:215–221. [PubMed: 2473557]

McCormick DA. Neurotransmitter actions in the thalamus and cerebral cortex and their role in neuromodulation of thalamocortical activity. Prog Neurobiol. 1992; 39:337–388. [PubMed: 1354387]

McCormick DA, Prince DA. Acetylcholine induces burst firing in thalamic reticular neurones by activating a potassium conductance. Nature. 1986; 319:402–405. [PubMed: 2418361]

McCormick DA, Bal T. Sleep and arousal: thalamocortical mechanisms. Annu Rev Neurosci. 1997; 20:185–215. [PubMed: 9056712]

Miwa JM, Freedman R, Lester HA. Neural systems governed by nicotinic acetylcholine receptors: emerging hypotheses. Neuron. 2011; 70:20–33. [PubMed: 21482353]

Oda S, Sato F, Okada A, Akahane S, Igarashi H, Yokofujita J, Yang J, Kuroda M. Immunolocalization of muscarinic receptor subtypes in the reticular thalamic nucleus of rats. Brain Res Bull. 2007; 74:376–384. [PubMed: 17845913]

Parent M, Descarries L. Acetylcholine innervation of the adult rat thalamus: distribution and ultrastructural features in dorsolateral geniculate, parafascicular, and reticular thalamic nuclei. J Comp Neurol. 2008; 511:678–691. [PubMed: 18924144]

Perkins KL. Cell-attached voltage-clamp and current-clamp recording and stimulation techniques in brain slices. J Neurosci Methods. 2006; 154:1–18. [PubMed: 16554092]

Pinault D. The thalamic reticular nucleus: structure, function and concept. Brain Res Brain Res Rev. 2004; 46:1–31. [PubMed: 15297152]

Ren J, Qin C, Hu F, Tan J, Qiu L, Zhao S, Feng G, Luo M. Habenula “cholinergic” neurons co-release glutamate and acetylcholine and activate postsynaptic neurons via distinct transmission modes. Neuron. 2011; 69:445–452. [PubMed: 21315256]

Sarter M, Parikh V, Howe WM. Phasic acetylcholine release and the volume transmission hypothesis: time to move on. Nat Rev Neurosci. 2009; 10:383–390. [PubMed: 19377503]

Scanziani M, Salin PA, Vogt KE, Malenka RC, Nicoll RA. Use-dependent increases in glutamate concentration activate presynaptic metabotropic glutamate receptors. Nature. 1997; 385:630–634. [PubMed: 9024660]

Sun YG, Wu CS, Renger JJ, Uebele VN, Lu HC, Beierlein M. GABAergic synaptic transmission triggers action potentials in thalamic reticular nucleus neurons. J Neurosci. 2012; 32:7782–7790. [PubMed: 22674255]

Szapiro G, Barbour B. Multiple climbing fibers signal to molecular layer interneurons exclusively via glutamate spillover. Nat Neurosci. 2007; 10:735–742. [PubMed: 17515900]

Tallini YN, Shui B, Greene KS, Deng KY, Doran R, Fisher PJ, Zipfel W, Kotlikoff MI. BAC transgenic mice express enhanced green fluorescent protein in central and peripheral cholinergic neurons. Physiol Genomics. 2006; 27:391–397. [PubMed: 16940431]

Wu CS, Zhu J, Wager-Miller J, Wang S, O'Leary D, Monory K, Lutz B, Mackie K, Lu HC. Requirement of cannabinoid CB(1) receptors in cortical pyramidal neurons for appropriate development of corticothalamic and thalamocortical projections. Eur J Neurosci. 2010; 32:693–706. [PubMed: 21050275]

Yamasaki M, Matsui M, Watanabe M. Preferential localization of muscarinic M1 receptor on dendritic shaft and spine of cortical pyramidal cells and its anatomical evidence for volume transmission. J Neurosci. 2010; 30:4408–4418. [PubMed: 20335477]

Yarosh CA, Acosta CG, Ashe JH. Modification of nicotinic ganglionic transmission by muscarinic slow postsynaptic potentials in the in vitro rabbit superior cervical ganglion. Synapse. 1988; 2:174–182. [PubMed: 2844002]

Zhang M, Wang YT, Vyas DM, Neuman RS, Bieger D. Nicotinic cholinoceptor-mediated excitatory postsynaptic potentials in rat nucleus ambiguus. Exp Brain Res. 1993; 96:83–88. [PubMed: 8243587]

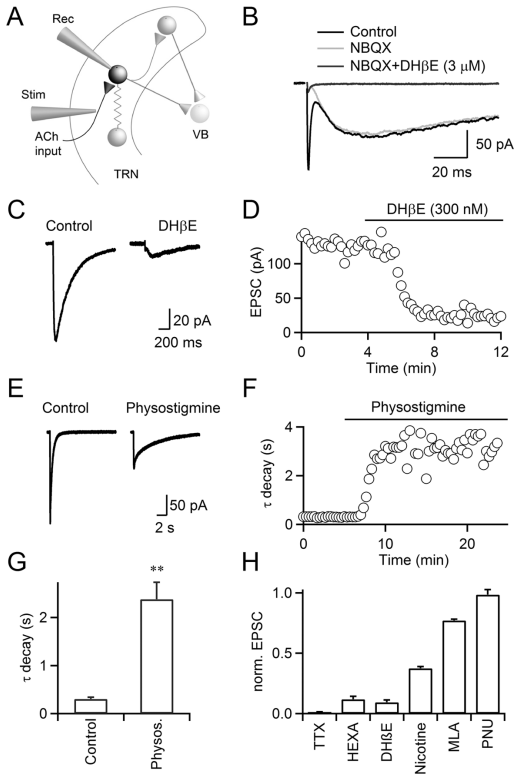

Figure 1. Cholinergic synaptic transmission in the TRN is mediated by α4β2 nAChRs

A, TRN neuronal circuit. TRN neurons were recorded with a Cs-based internal solution. Synaptic inputs were activated with a patch pipette (Stim), placed at lateral distances of 100–200 μm. VB, ventrobasal thalamus; Rec, recording pipette; Stim, stimulus electrode. **B**, For a representative experiment, single stimuli evoked EPSCs with a fast and a slow component (black trace) in a TRN neuron. The fast component was blocked by the AMPAR antagonist NBQX (10 μM, grey trace), and the slow component was blocked by the nAChR antagonist DHβE (3 μM, dark grey trace). **C, D**, A representative experiment showing that nEPSCs were blocked by low doses of DHβE (300 nM, **C**). Time course of nEPSC amplitude during bath application of DHβE (300 nM), for the same cell (**D**). **E, F**, A representative experiment showing that application of the acetylcholinesterase (AChE) inhibitor physostigmine (10 μM) prolonged nEPSC decay and reduced nEPSC amplitude (**E**). Time course of nEPSC decay during bath application of physostigmine (10 μM, **F**). Decay was fit by a single exponential function. Experiment was carried out in the presence of atropine (10 μM). **G**, Summary showing that physostigmine (10 μM) increased time constant of nEPSC decay. $n = 5$, ** $p < 0.01$. Paired Student's *t*-test. **H**, Summary showing the effect of TTX (500 nM), hexamethonium (HEXA, 100 μM), DHβE (300 nM), nicotine (100 nM), methyllycaconitine (MLA, 50 nM), PNU 120596 (PNU, 10 μM) on nEPSC amplitude, normalized to control. $n = 5–8$.

Sun et al.

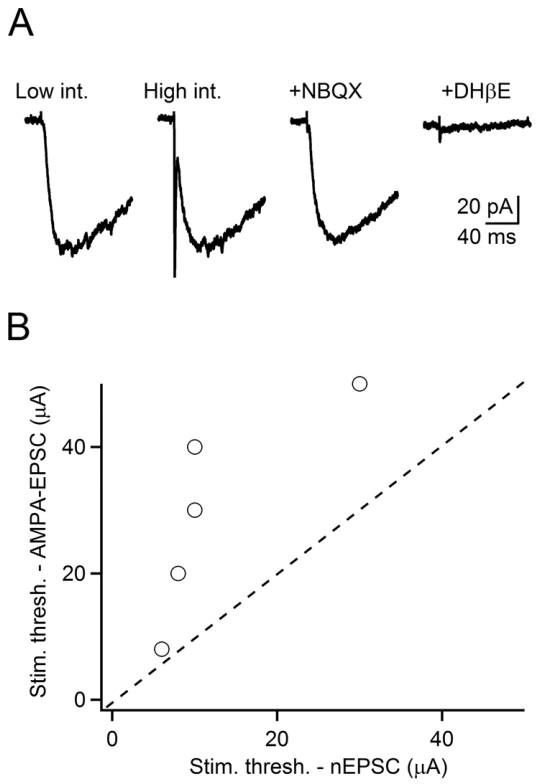

Figure 2. Glutamate and ACh are released from distinct sets of synapses

TRN neurons were recorded in voltage clamp with a Cs-based internal solution in the presence of R-CPP, picrotoxin, and CGP55845 to block NMDA, $GABA_A$, and $GABA_B$ receptors, respectively. (**A**) Representative recording showing that low intensity stimuli trigger nEPSCs, blocked by DHβE (3 μM). Increases in stimulus intensity led to the recruitment of AMPAR EPSCs, blocked by NBQX (10 μM), while the nEPSC amplitude remained unchanged. (**B**) Summary plot showing distinct thresholds for AMPAR- and nEPSCs. $n = 5$.

Sun et al.

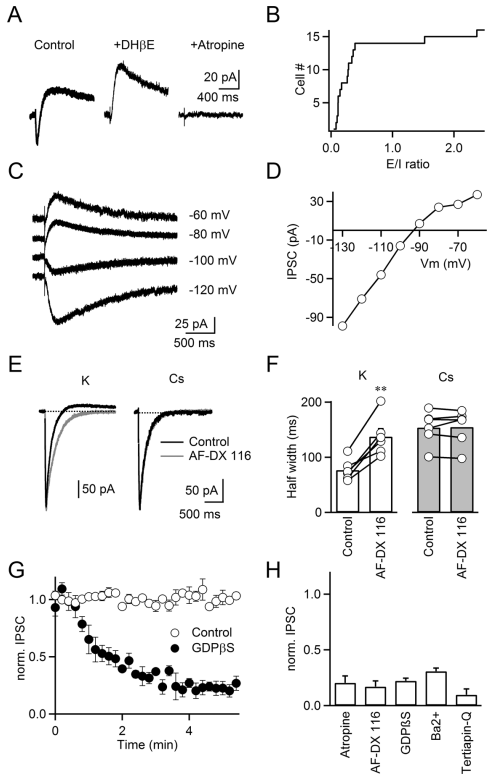

Figure 3. Synaptic activation of M2 mAChRs evokes IPSCs mediated by GIRK

TRN neurons were recorded with a K-based internal solution, except in (**E**, **F**). **A**, Biphasic (E-I) postsynaptic response in a TRN neuron, with inward current blocked by the nAChR antagonist DHβE (3 μM). The remaining outward current was blocked by the mAChR antagonist atropine (10 μM). **B**, Plot of the cumulative distribution of E/I ratios (n = 17 experiments). For biphasic responses, `E' was defined as the current integral between nEPSC onset and zero crossing (inward current). `I' was defined as the current integral following the zero crossing (outward current). **C, D**, IPSCs display inward rectification. IPSCs were evoked for a range of different holding potentials (**C**). IPSC amplitudes are plotted against membrane potential for the same neuron (**D**). **E**, Representative experiments showing cholinergic postsynaptic currents recorded with a K-based internal solution (left) or Cs-based internal solution (right), under control condition (black traces) and following application of AF-DX 116 (10 μM, grey traces). **F**, Summary data plot half width of the nEPSC recorded with a K-based internal solution (left) or a Cs-based internal solution (right), prior to and following AF-DX 116 (10 μM) application. **, $p < 0.01$, paired Student's t-test. $n = 6$. **G**, In TRN neurons recorded with an internal solution supplemented with GDPβS (1 mM), isolated muIPSC amplitude strongly attenuated following establishment of whole-cell configuration at t = 0 (filled circles). Control (open circles) shows recordings without GDPβS. Experiments were carried out in the presence of hexamethonium (100 μM) to block nEPSC. $n = 6–7$. **H**, Summary showing the effect of atropine (10 μM), AF-DX 116 (10 μM), GDPβS (1 mM), Ba^{2+} (200 μM), Tertiapin-Q (200 nM) on the isolated muIPSC amplitude, normalized to control. For Tertiapin-Q experiments, cells were held at ~-105 mV to measure inward currents. $n = 5–7$.

Sun et al.

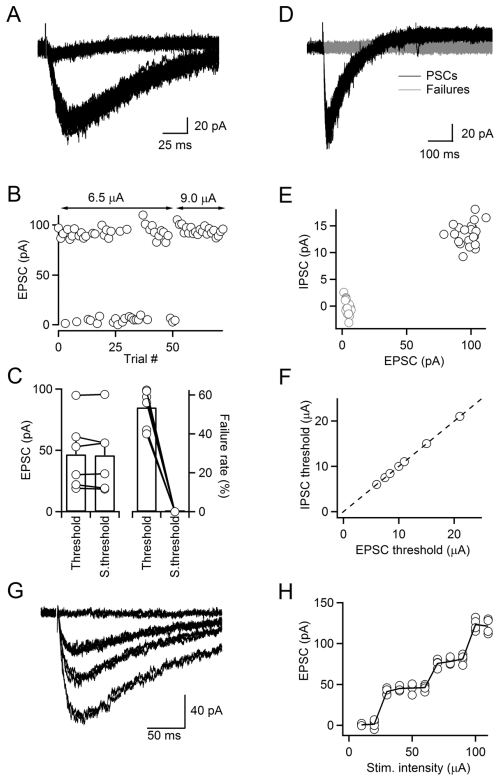

Figure 4. Release of ACh from individual cholinergic axons activates both nAChRs and mAChRs

A–C, Minimal stimulation of cholinergic inputs. TRN neurons were recorded with a Cs-based internal solution. A representative experiment shows overlay of 50 individual trials, including both failures and nEPSCs, evoked at a fixed stimulus intensity (6.5 μA, **A**). For the same neuron, increases in stimulus intensity from 6.5 μA to 9.0 μA resulted in elimination of failures, while the amplitude of nEPSCs in successful trials remained unchanged (**B**). Summary plot showing that unitary nEPSC amplitude did not change following increase in stimulus intensity ($p = 0.58$, left panel, **C**). For the same increase in stimulus intensity, failure rate decreased from 53.5% to 0 ($p < 0.001$, right panel, **C**, $n = 6$ cells). **D–F**, ACh release from individual axons activates both nAChRs and mAChRs. TRN neurons were recorded with a K-based internal solution. Representative experiment shows that stimulation of an individual cholinergic fiber at threshold elicits trials with both nEPSCs and muIPSCs or failures as shown by overlay of individual trials, evoked for a fixed stimulus intensity (8.4 μA, **D**). Graph shows muIPSC amplitude plotted against nEPSC amplitude for individual trials at threshold (**E**), same data as shown in (**D**). Summary plot showing the threshold stimulus intensity necessary to evoke nEPSC and muIPSC. Each point represents data from an individual experiment (**F**, $n = 7$). **G, H**, A representative experiment showing nEPSCs (averages of 4–5 individual trials) evoked by a series of stimulus intensities (10–110 μA, 10 μA steps, **G**). For the same neuron, graph plots nEPSC amplitudes evoked in individual trials as a function of stimulus intensity (**H**). Neurons were recorded with a Cs-based internal. S.threshold, suprathreshold.

Sun et al.

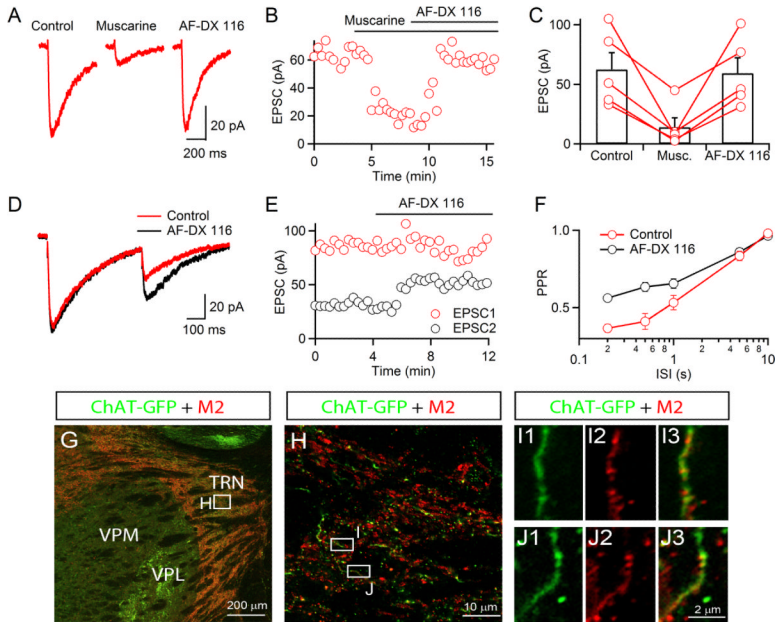

Figure 5. Autoinhibition of ACh release is mediated by presynaptic M2 mAChRs

Recordings were carried out with a Cs-based internal solution. **A**, A representative experiment showing nEPSC suppression by bath application of muscarine (1 μM), reversed by the M2 antagonist AF-DX 116 (10 μM). **B**, For the same neuron, graph plots time course of nEPSC amplitude prior to and following application of muscarine and AF-DX 116. **C**, Summary data showing nEPSC suppression by muscarine (1 μM), reversed by AF-DX 116 (10 μM). $n = 5$. **D**, nEPSCs evoked by paired stimuli (500 ms ISI) prior to (red) and following application of the M2 mAChR antagonist AF-DX 116 (10 μM, black) in a representative recording. **E**, Time course of $EPSC_1$ (red circles) and $EPSC_2$ (black circles) prior to and during application of AF-DX 116 (10 μM) for the same neuron as in (**D**). **F**, Summary showing $EPSC_2/EPSC_1$ (PPR) for different inter-stimulus intervals (ISI) in control (red circles) and AF-DX 116 (black circles). $n = 5$. **G**, Immunohistochemical staining in ChAT-GFP reporter mice indicates strong expression of M2 mAChRs in the TRN. Expression of ChAT-GFP was labeled by antibodies against GFP (green) and M2 mAChRs were detected by antibodies against M2 mAChRs (red). **H**, Higher magnification view for the area indicated in **G**, showing M2 mAChR is partially overlapping with GFP signal in the TRN. **I,J**, Examples showing higher magnification views of the areas indicated in **H**. M2 mAChR positive signals (red, **I2,J2**) colocalize with GFP positive signal (green, **I1,J1**), as shown in the overlay in **I3, J3**. VPM, ventral posteromedial nucleus of thalamus; VPL, ventral posterolateral nucleus of thalamus.

Sun et al.

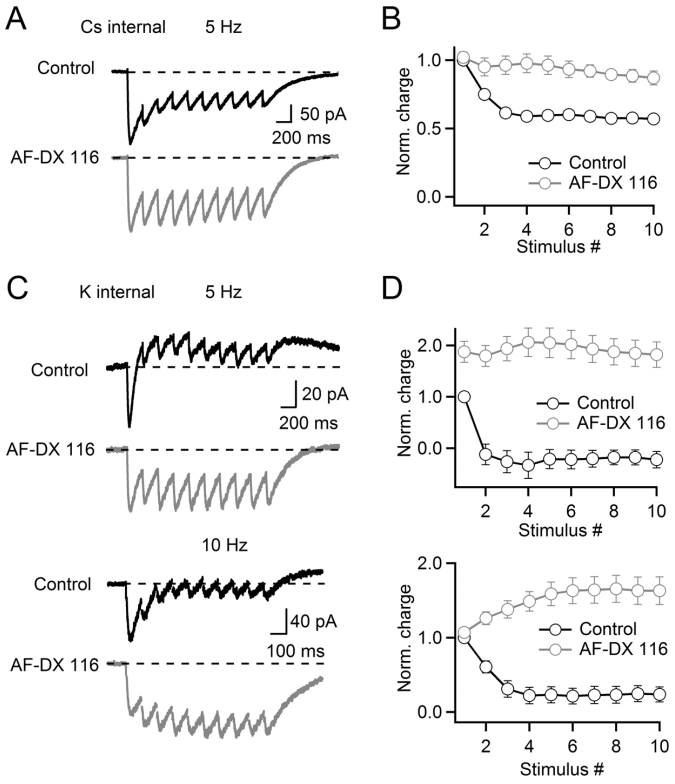

Figure 6. Pre- and postsynaptic muscarinic receptors control cholinergic signaling during brief stimulus trains

Recordings in (**A–B)** were done with a Cs-based internal solution, for (**C–D**) a K-based internal solution was used. **A**, A representative experiment showing nEPSCs in response to a train of stimuli (5 Hz, 10 pulses) in control (black trace) and after bath application of AF-DX 116 (10 μM, grey trace). **B**, Summary data, plotting synaptic charge (measured as the area underneath the voltage trace) following each stimulus, normalized to the first EPSC in control (control, black circles; AF-DX 116, grey circles). $n = 5$ cells. **C**, Rapid suppression of nAChR-evoked excitation by mAChR activation, blocked by AF-DX 116. Representative experiments showing PSCs in response to trains of stimuli at 5 Hz or 10 Hz, in control (black traces) and after bath application of AF-DX 116 (10 μM, grey traces). **D**, Summary data, plotting net synaptic charge (measured as the area underneath the voltage trace) following each stimulus at 5 Hz or 10 Hz, normalized to the net synaptic charge evoked by the first PSC in control (control, black circles; AF-DX 116, grey circles). $n = 8$ cells for both frequencies.

Sun et al.

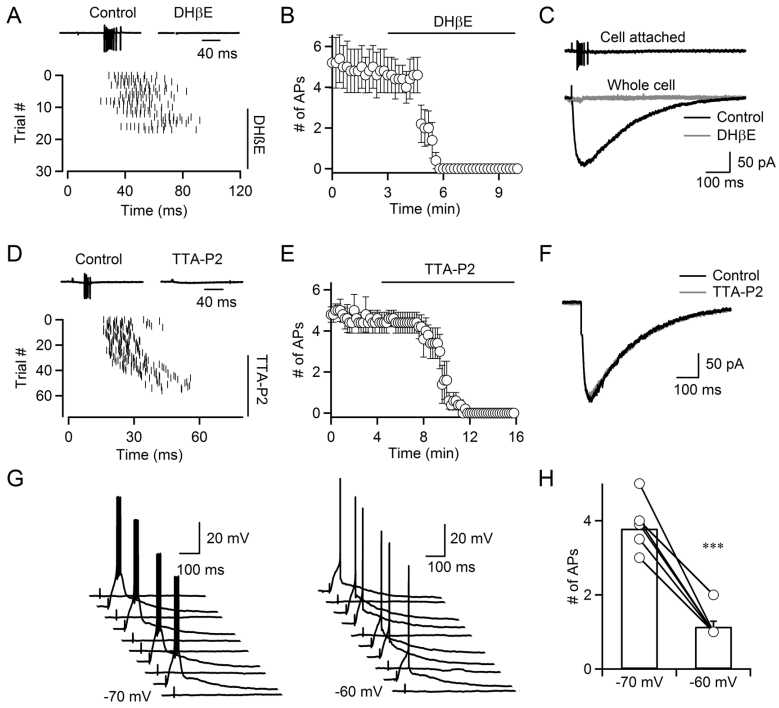

Figure 7. Cholinergic synaptic inputs trigger action potentials in TRN neurons

A, Top: Synaptically evoked action potentials in a TRN neuron recorded in loose-patch mode, blocked by application of DHβE (300 nM). Bottom: Raster plot showing the timing of spikes evoked by single stimuli applied at t = 0 ms, prior to and during bath application of DHβE (300 nM). **B**, Time course of DHβE-induced block of synaptically evoked action potential firing (*n* = 5 neurons). **C**, Top: Single stimulus elicits burst of action potentials in a TRN neuron recorded in cell-attached configuration, using a Cs-based internal solution. Bottom: For the same neuron recorded in whole cell voltage clamp, stimulation at the same intensity evoked a nEPSC that was completely blocked by DHβE (300 nM). **D**, Top: Synaptically evoked action potentials in a TRN neuron recorded in loose-patch mode, blocked by the specific T-type Ca^{2+} channel antagonist TTA-P2 (1 μM). Bottom: Raster plot showing the timing of spikes evoked by single stimuli applied at t = 0 ms, prior to and during bath application of TTA-P2 (1 μM). **E**, Summary data showing the time course of the TTA-P2-induced block of synaptically evoked action potential firing in TRN neurons (*n* = 5 neurons). **F**, ACh release is not influenced by TTA-P2. A representative experiment showing a nEPSC in control (black) and following bath application of TTA-P2 (1 μM, grey). TRN neurons were recorded in whole-cell voltage clamp with a Cs-based internal solution. Traces are averages of 20–30 individual trials. **G,H**, Resting membrane potential determines ACh-induced spiking in TRN neurons. Neurons were recorded in current clamp with a K-based internal solution. A representative experiment shows trials with response successes and failures, evoked by fixed stimulus intensity, indicating activation of a single cholinergic axon (**G**). Bursts were evoked at a holding potential of −70 mV (**G**, left), and single spikes at a holding potential of −60 mV (**G**, right). Summary plot showing that cholinergic synaptic inputs trigger action potentials in a state-dependent manner (**H**). Data include single- and multiple fiber responses. *** p<0.001, paired Student's t-test. *n* = 7.
Sun et al.

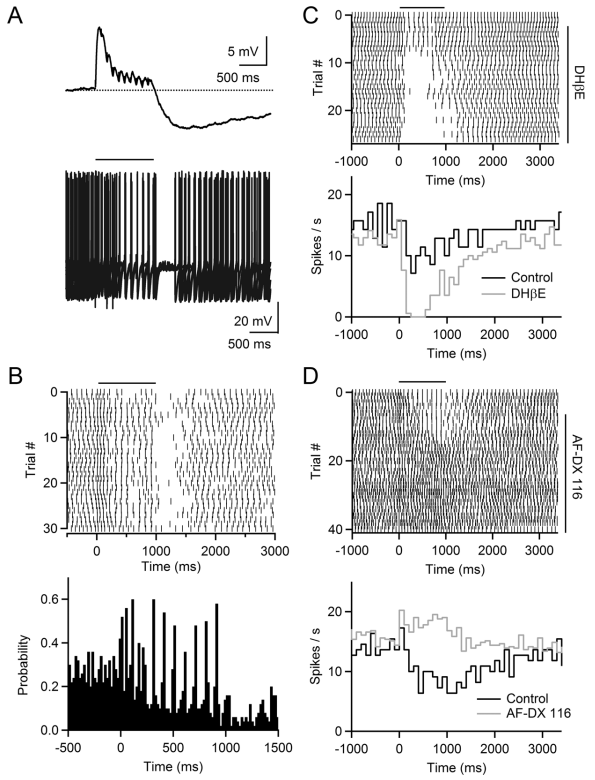

Figure 8. Cholinergic synaptic inputs entrain TRN neuronal activity

Neurons were recorded with a K-based internal solution and held in current clamp. **A**, Top: Postsynaptic E-I response evoked by a brief stimulus train (10 stimuli, 10 Hz), for a TRN neuron held at −60 mV. Bottom: The same stimulus train (indicated by horizontal bar) was applied during ongoing action potential activity evoked by depolarizing current steps (6 s, 120 pA). Shown are 5 consecutive trials. **B**, Top: Raster plot showing the timing of spikes in consecutive trials during and following stimulus train (onset of synaptic stimulation at t = 0 ms), for same cell as shown in (**A**) Bottom: Poststimulus time histogram (PSTH, bin size = 20 ms), compiled for 58 consecutive trials. **C**, In a different neuron, spike entrainment to cholinergic stimulation was eliminated by blocking nAChRs. Top: Raster plot showing timing of spikes during stimulus train (10 stimuli, 10Hz), prior to and following bath application of the nAChR antagonist DHβE (3 μM). Bottom: PSTH (bin size = 100 ms), for spike firing in control (black), and following bath application of DHβE (grey). **D**, Block of spike entrainment by pharmacological block of M2 muscarinic receptors. Top: Raster plot showing timing of spikes during stimulus train (10 stimuli, 10Hz), prior to and following bath application of the mAChR antagonist AF-DX 116 (10 μM). Bottom: PSTH (bin size = 100 ms), for spike firing in control (back), and following bath application of AF-DX 116 (grey).

Sun et al.